# Innovative synthesis of mesostructured CoSb 3 -based skutterudites by magnesioreduction

S. Le Tonquesse, E Alleno, Valérie Demange, V. Dorcet, Loïc Joanny, C. Prestipino, O. Rouleau, M. Pasturel

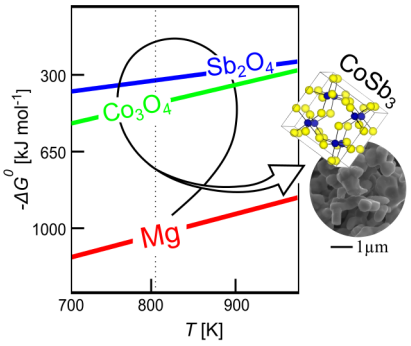

# Innovative synthesis of mesostructured $CoSb_3$-based skutterudites by magnesioreduction

Sylvain Le Tonquesse[a], Éric Alleno[b], Valérie Demange[a], Vincent Dorcet[a], Loic Joanny[a], Carmelo Prestipino[a], Olivier Rouleau[b], Mathieu Pasturel[a,*]

[a]*Univ Rennes, CNRS, ISCR-UMR6226/ScanMAT-UMS2001, F-35000, Rennes, France*
[b]*Université Paris-Est, Institut de Chimie et des Matériaux Paris-Est, UMR 7182 CNRS - UPEC, 2 rue H. Dunant, 94320 THIAIS, France*

**Abstract**

High purity $CoSb_3$, $Ni_{0.06}Co_{0.94}Sb_3$ and $In_{0.13}Co_4Sb_{12}$ were synthesized from oxides by magnesioreduction. This novel synthesis route to $CoSb_3$-based skutterudites directly yields highly cristalline powders with submicronic grain size. Densified mesostructured pellets with an average grain size ranging between 550 and 800 nm were obtained by spark plasma sintering. The strong phonon scattering induced by the mesostructuration leads to a lattice thermal conductivity reduction up to 25 % for $CoSb_3$ and $Ni_{0.06}Co_{0.94}Sb_3$ at 300 K without significantly degrading the electronic properties. Consequently, maximum *ZT* figures-of-merit of 0.09, 0.60 and 0.75 are found for $CoSb_3$, $Ni_{0.06}Co_{0.94}Sb_3$ and $In_{0.13}Co_4Sb_{12}$, respectively, showing the ability of this scalable process to reach the best performances reported in literature for these compositions at moderate temperature and annealing duration.

*Keywords:* Intermetallics; Thermoelectic materials; Chemical synthesis; Powder metallurgy; Microstructure

*mathieu.pasturel@univ-rennes1.fr

# 1. Introduction

Thermoelectric materials (TM) enable the direct conversion of a temperature gradient into voltage, thus offering the opportunity to directly exchange wasted heat into electricity by highly reliable solid state power generators. However, TM-based technologies are still only used in niche applications because of the low performances, high cost or complex synthesis of the currently available materials [1]. Among them, $CoSb_3$-based skutterudites have attracted great attention as promising mid-temperature TM due to their high power factor $PF = \alpha^2/\rho$ (where $\alpha$ is the Seebeck coefficient and $\rho$ the electrical resistivity), good mechanical properties and relatively abundant constituting chemical elements [2, 3, 4, 5]. However its thermal conductivity $\kappa$ is high - up to 9 W $m^{-1}$ $K^{-1}$ at 293 K in polycristalline $CoSb_3$ [6] - mainly due to the lattice (phonon) contribution $\kappa_L$ and much less to the charge carrier contribution $\kappa_e$, with $\kappa = \kappa_L + \kappa_e$.

Any attempt to improve the dimensionless thermoelectric figure-of-merit $ZT$, defined as:

$$ZT = \frac{\alpha^2}{\rho(\kappa_L + \kappa_e)}T \tag{1}$$

in $CoSb_3$ involves (i) the optimization of $PF$ by adjusting the carrier concentration in the semiconducting material and (ii) the reduction of $\kappa_L$. The latter can be achieved by creating phonon scattering centers at different length scales in the materials:

(i) At the atomic scale, the most common strategy consists in partially filling the icosahedral *2a* crystallographic position of skutterudite structure with heavy atoms. The low energy phonons introduced by the filler atom as well as the mass fluctuation arising from its random occupancy both scatter the heat carrying phonons resulting in a strongly reduced $\kappa_L$ [7, 8, 9, 10]. Chemical doping on the Co- or Sb-sublattice, which is necessary to achieve optimal charge carrier concentration, has also been shown to affect the thermal conductivity via the mass fluctuation phenomenon [11, 12].

(ii) At the microstructural scale, grain boundaries in bulk polycrystalline materials also act as effective phonon-scattering centers [13, 14]. Their effect is highly intensified in nano- or mesostructured materials where $\kappa_L$ can be reduced by more than 35 % compared to identical materials with much larger grain size [15, 16]. As a result, it stimulates the development of alternative synthesis routes more suitable for the production of submicronic powders than traditional melting-annealing methods, such as ball-milling / spark plasma sintering (SPS) [17, 18], severe plastic deformation [19], melt spinning [20, 21], combustion synthesis [22], flash-spark plasma sintering [23], high-pressure syntheses [24, 25], gas atomization [26] or solution proceed [27, 28]. Improvement of *ZT* by this approach can only be realized if the decrease of $\kappa$ is not counterbalanced by a decrease of *PF* due to overly enhanced electron scattering at the grain boundaries.

Phonons being more likely scattered by defects with sizes close to their wavelengths, the creation of defects at different length scales in the material, often refereed as 'all-scale hierarchical architectures', offers the possibility to scatter phonons over a broader energy spectrum, thus reducing $\kappa$ more efficiently [1, 29, 30, 31]. Very recently, this multi-scale approach have been successfully employed with nanostructured filled-skutterudites [32, 33], porous doped-skutterudites [34, 35] or formation of nanoinclusions in filled- and doped-skutterudites [36, 37].

With this approach in mind, we developed the magnesioreduction synthesis of pristine, Ni-doped and In-filled $CoSb_3$ according to the reaction:

$$\frac{1}{3}Co_3O_4 + \frac{3}{2}Sb_2O_4 + \frac{22}{3}Mg \xrightarrow[84\ h]{810\ K} CoSb_3 + \frac{22}{3}MgO \qquad (2)$$

This new synthesis route to $CoSb_3$-based skutterudites, inspired from industrial pyrometallurgical processes (*e.g.* Kroll's process), yields powders with submicronic grain size that can be readily used for the sintering of mesostructured densified materials [38]. It offers other advantages such as the use of air stable and cheap oxides as precursors, relatively low temperature and short reaction

time compared to conventional melting/annealing synthesis, good control of the chemical composition and high yield. In this article, the structural, microstructural and thermoelectric characterizations of these materials are reported and compared to literature data on similar materials (either mesostructured or not) prepared by conventional synthesis routes.

# 2. Experimental procedures

## 2.1. Synthesis of $CoSb_3$ by magnesioreduction

The first step of the synthesis consists in the preparation of an intimate mixture of $Co_3O_4$ (Sigma-Aldrich, 99.9 %) and $Sb_2O_4$ (Sigma-Aldrich, 99.995 %) with a molar ratio of 1:5.4 (20 % excess of $Sb_2O_4$) by thoroughly grinding the powders together in a vibrating mill (Retsch MM200) for 20 min at 25 Hz using tungsten carbide vial and ball. The oxide mixture was then cold-pressed at 250 MPa into Ø 10 mm pellets with approximately 2 mm height. Two pellets were stacked together on top of a Mg chips bed (Strem, $\geq$ 99 %) lying at the bottom of a Mo crucible (Fig. 1). The quantity of Mg needed to complete the reduction was determined from the masses of $Co_3O_4$ and $Sb_2O_4$ to be reduced plus an additional 2-3 % excess. The Mo crucible is then closed and placed in an argon-filled Inconel tube to prevent its oxidation during the thermal process. The reactor was heated up to 810 K at 100 K $h^{-1}$ and held at this temperature for 84 h before being cooled down to room temperature. After the reaction, $CoSb_3$ remains in the shape of compact pellets and could easily be separated from the loose MgO. The powders were spark plasma sintered (FCT HP-D-10 system) in Ø 10 mm graphite dies at 910 K and 66 MPa for 5 min with heating/cooling ramps of 100 K $min^{-1}$.

## 2.2. Synthesis of $Ni_{0.06}Co_{0.94}Sb_3$ and $In_{0.13}Co_4Sb_{12}$ by magnesioreduction

The synthesis of Ni-doped and In-inserted $CoSb_3$ was attempted from a mixture of cobalt, nickel/indium and antimony oxides. Nevertheless, the primary for-

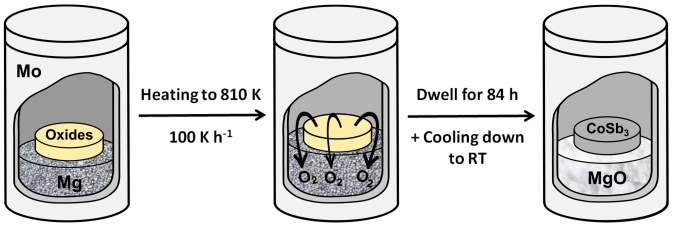


Fig. 1: Experimental procedure for the synthesis of $CoSb_3$-based skutterudites by magnesioreduction of the corresponding (un-)doped $Co_3O_4$ and $Sb_2O_4$ oxide precursors (yellow pellet). See text for details.

mation of $NiSb_2$ and InSb during the magnesioreduction process did not allow to obtain pure samples in relatively fast and low temperature conditions. Mixed precursor oxides were thus prepared in order to start from an intimate mixture of metallic ions to speed up the process.

For the preparation of $Ni_{0.18}Co_{2.82}O_4$ precursor, $Co(NO_3)_2.6H_2O$ (Fluka, $\geq$ 98%) and $Ni(NO_3)_2.6H_2O$ (Fluka, $\geq$ 99%) were dissolved in distilled water with a molar ratio of about 16:1. The solution was stirred for 30 min and evaporated at 363 K. The slurry was ground before being decomposed in air at 573 K for 4 h leading to the formation of a black powder. The Bragg peaks of the X-ray diffraction (XRD) patterns correspond to the $Co_3O_4$ structure ($Fd\bar{3}m$) with lattice parameter $a = 8.0905(5)$ Å (Fig. SI.1), suggesting the insertion of Ni in $Co_3O_4$ ($a \approx 8.086$ Å). Accordingly, the metal ratio determined by X-ray energy dispersive spectroscopy (EDS) is in good agreement with the expected $Ni_{0.18}Co_{2.82}O_4$ composition.

For the preparation of $In_{0.10}Co_{2.90}O_4$ precursor, $CoCl_2.6H_2O$ (Prolabo, 99.9 %) and $In(NO_3)_3.xH_2O$ (home made by dissolving metallic indium in concentrated nitric acid) were dissolved in distilled water with a molar ratio of about 29:1 under vigorous stirring. Then a suitable amount (+20 % excess) of NaOH was added to form the metal hydroxides. The blue precipitate was then centrifuged, washed with water and ethanol, dried overnight at about 363 K and calcinated at 723 K to obtain the corresponding oxide. Powder XRD pattern (Fig. SI.2) shows broad diffraction peaks corresponding to the $Co_3O_4$ structure. Le Bail

refinement of the experimental pattern nevertheless converges to a cell parameter $a = 8.102(7)$ Å which could indicate the insertion of In on the Co-lattice in agreement with recent results by Ma *et al.* [39].

From these $Ni_{0.18}Co_{2.82}O_4$ and $In_{0.10}Co_{2.90}O_4$ precursors, $Ni_{0.06}Co_{0.94}Sb_3$ and $In_{0.13}Co_4Sb_{12}$ were synthesized using the same procedure as for $CoSb_3$, at identical temperature and duration.

These compositions have been selected as (i) the optimized carrier concentration for Ni-doped sample [40, 41] and as (ii) a composition close to those usually presented in articles dealing with In-inserted skutterudites [42, 43, 44, 45, 46, 47].

## 2.3. Materials characterization

The crystal structure and purity of the samples were checked by powder XRD using a Bruker D8 Advance diffractometer in the Bragg-Brentano geometry working with a monochromatized Cu K$\alpha_1$ radiation ($\lambda = 1.5406$ Å). The diffractometer is equipped with a 1D LynxEye detector with a photon energy discrimination around 20 % thus reducing the cobalt fluorescence signal. Lattice constants were determined by Le Bail refinements as implemented in the FullProf Suite software [48].

Scanning electron microscopy (SEM) images, energy dispersive spectroscopy (EDS) and electron backscattering diffraction (EBSD) were performed using a JEOL JSM 7100 F microscope equipped with an Oxford EDS SDD X-Max spectrometer and an EBSD HKL Advanced Nordlys Nano detector. Preparation of the powder samples for SEM analyses consisted in a mere deposition on carbon tape followed by metallization with carbon. As for the densified samples, the pellets were successively polished with SiC, diamond paste and colloidal silica and pasted on SEM holders using silver lacquer. Samples for the transmission electron microscopy were first thinned by dimpling with colloidal silica and then by Ar ion milling using a Fischione Ion Mill 1010 operating at 4.5 kV and 5 mA. Transmission electron microscopy (TEM) analyses were performed on a JEOL 2100 $LaB_6$ instrument operating at 200 kV and equipped with a high resolution

Gatan US1000 camera, and an Orius 200D camera.

The Seebeck coefficient $\alpha$(T) and electrical resistivity $\rho$(T) measurements were realized using a home made apparatus described elsewhere [49]. Thermal diffusivities were measured in argon atmosphere with the laser flash method using a Netzsch LFA 457 equipment. The total thermal conductivity $\kappa$ was determined by multiplying the thermal diffusivity, the specific heat calculated from the Dulong-Petit law and the experimental density of the samples.

# 3. Results and discussion

## 3.1. Structural and microstructural characterization of as-synthesized and SPSed materials

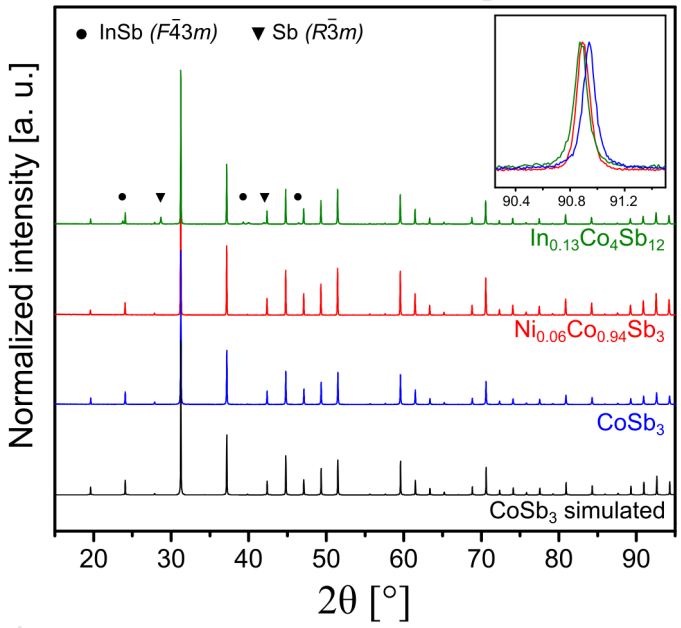


Fig. 2: Experimental XRD patterns of the as-synthesized skutterudite powders and theoretical one calculated with FullProf [48] from cell parameters and atomic positions given in [50] and peak profile function from the utilized diffractometer. The inset shows the shift of the (653) diffraction peak of the $CoSb_3$ structure (systematic peak shift due to sample displacement is corrected) revealing the lattice parameter evolution among the samples.

The powder XRD patterns of pristine and Ni-doped $CoSb_3$ (Fig. 2) are fully

indexed according to the skutterudite structure, revealing a single phase product. Only few traces of InSb ($F\bar{4}3m$) and Sb ($R\bar{3}m$) are visible on the XRD pattern of the indium containing compound. Le Bail fitting of the XRD patterns results in cell parameters of $a$ = 9.0350(2), 9.0434(1) and 9.0443(6) Å for $CoSb_3$, $Ni_{0.06}Co_{0.94}Sb_3$ and '$In_{0.13}Co_4Sb_{12}$', respectively, indicating an effective substitution by nickel on the cobalt site and insertion of indium in the cages of the structure [44, 51, 52]. By comparison with literature data, one can expect chemical compositions close to $Ni_{0.06}Co_{0.94}Sb_3$ and $In_{0.10}Co_4Sb_{12}$ from these lattice parameter values [40, 53]. The discrepancy with the targeted In-concentration could be explained by some residual InSb binary compound in the sample. The diffraction peaks exhibit very narrow profiles characteristic of well-crystallized matter which may favor the electrical transport in these materials. Surprisingly, no traces of MgO are visible on these patterns which is quite unusual for such a process [54, 55, 56] and may result either from the absence of this by-product or from its amorphous nature, the reaction being carried out at a relatively low temperature.

SEM examination of the obtained powders reveals faceted submicronic grains (Fig. 3). The grain size ranges from 300 nm to 1 $\mu$m for $CoSb_3$ and its Ni-doped counterpart and from 100 nm to 1 $\mu$m for the In-inserted skutterudite. Such small particles are required to lower the thermal conductivity and are usually obtained by high energy ball-milling with both risks of contamination from the milling material and decomposition of the phase. In agreement with the narrow XRD peaks, the shape of most of the grains clearly indicates their single crystalline nature. EDS analyses of the Ni-doped $CoSb_3$ powders confirm the presence of Ni in the sample with a concentration of $\approx$ 1 at.%. On the other hand, no characteristic X-ray emission peaks of In could be detected for the filled skutterudite and this could be explained by the low concentration of the element in the material ($<$ 1 at.%) being below the detection limit of the technique. No signal of Mg is visible on the X-ray emission spectra from all the samples.

Both XRD and EDS analyses indicate the absence of MgO in the as-synthesized

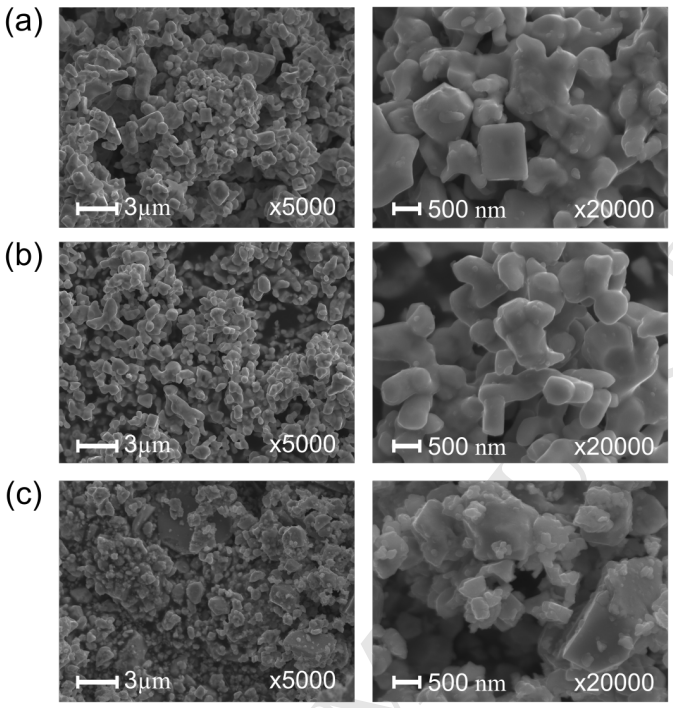


Fig. 3: Secondary electron SEM images of the as-synthesized (a) $CoSb_3$ (b) $Ni_{0.06}Co_{0.94}Sb_3$ and (c) $In_{0.13}Co_4Sb_{12}$ at two different magnifications.

products. In addition, TEM observations coupled with EDS analyses did not reveal any traces of Mg or MgO particles in the samples. Together with the retention of both mixed-oxide pellet and magnesium turning shapes, and based on the Ellingham diagram [57] for the metals in presence, we hypothesize solid-gas driven reduction reactions at 810 K: Mg consumes the residual $O_2$ atmosphere in the crucible ($p_{eq}(O_2) = 10^{-63}$ Pa) inducing the decomposition of $Co_3O_4$ ($p_{eq}(O_2) = 10^{-19}$ Pa) and $Sb_2O_4$ ($p_{eq}(O_2) = 10^{-14}$ Pa) into native metals that readily react together to form the skutterudite phase.

Spark plasma sintering was used to prepare the skutterudite pellets because it can achieve high densities in short sintering times thus limiting grain growth during the densification process. With the sintering conditions given in 2.1, relative densities ranging from 96 to 97 % were obtained (Table 1).

Le Bail fitting of the XRD patterns measured on sintered pellets polished

surfaces (Fig. 4 and SI.4) do not show significant evolution of the unit cell parameter for $CoSb_3$ and $Ni_{0.06}Co_{0.94}Sb_3$ ($a$ = 9.0361(2) and 9.0428(1) Å, respectively). A significant increase up to $a$ = 9.0482(3) Å is observed for $In_{0.13}Co_4Sb_{12}$, which, together with the disappearance of the InSb Bragg peaks, is attributed to a higher insertion of indium in the cages available in the skutterudite structure. Considering the low melting point (789 K) reported for InSb [58], its reactivity with the skutterudite matrix during the sintering process performed above this melting point was expected. Only a very small amount of antimony ($R\bar{3}m$) could be detected by XRD after sintering and it was found to represent less than 1 wt.% of the sample. The latter cell parameter corresponds to the composition $In_xCo_4Sb_{12}$ with $0.13 \leq x \leq 0.15$, depending on the literature data [42, 53].

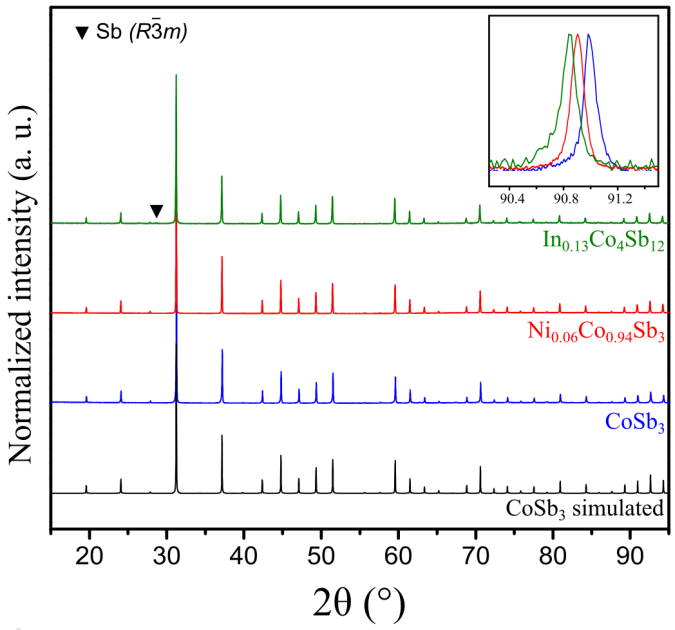


Fig. 4: Experimental XRD patterns of the sintered skutterudite pellets and theoretical one calculated with FullProf [48] from cell parameters and atomic positions given in [50] and peak profile function from the utilized diffractometer. The inset shows the shift of the (653) diffraction peak of the $CoSb_3$ structure (systematic peak shift due to sample displacement is corrected) revealing the lattice parameter evolution among the samples.

SEM-EDS analyses performed on several spots of the polished surfaces gives

a mean Ni concentration of 1.5 at.% for the Ni-doped samples, which is in good agreement with the targeted and crystallographic compositions. This composition is homogeneous through the analyzed polished surface and no concentration gradient is observed. As for the powders, no significant In or Mg content could be detected on any samples by EDS analyses which means that those elements are in concentration below the detection limit of the technique.

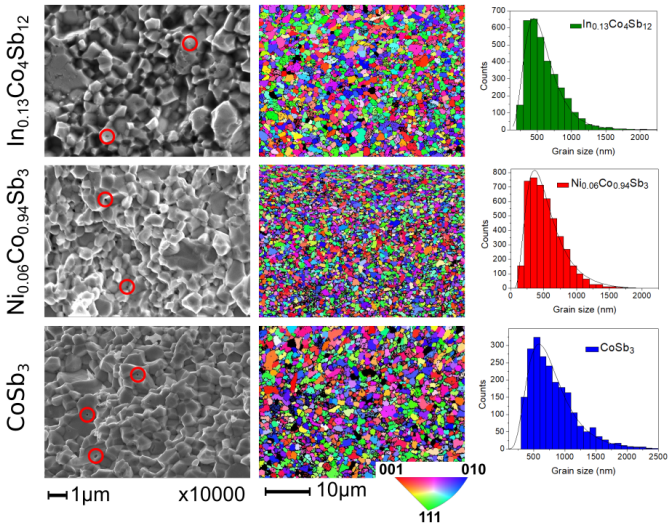


Fig. 5: Secondary electron SEM images of the pellet cross-sections (left) showing some residual porosity (circled in red). EBSD mappings (middle) of the polished pellet surfaces and histograms (right) showing the distribution of grain sizes determined from EBSD maps for the SPSed $CoSb_3$ (bottom), $Ni_{0.06}Co_{0.94}Sb_3$ (middle) and $In_{0.13}Co_4Sb_{12}$ (top) skutterudites.

In order to check how sintering affects grain size, electron backscattering diffraction (EBSD) and SEM imaging (Fig. 5) were performed on polished surfaces and on broken cross-sections of the pellets, respectively. SEM imaging reveals some closed porosity (encircled in red) which is responsible for the full densification deviation. EBSD mappings were realized on a 1750.5 $\pm$ 9.5 $\mu m^2$ area with a step size of 100 nm for $CoSb_3$ and $In_{0.13}Co_4Sb_{12}$ and 50 nm for $Ni_{0.06}Co_{0.94}Sb_3$ to distinguish better smaller grains. Kikuchi lines were well indexed using the skutterudite structure and cell parameters obtained from XRD, and only a few non-indexed areas were found on the 3 pellets. First of all, one

can notice a random distribution of the grains orientation throughout the analyzed areas. Then submicronic particles are found to cover the majority of the surface in all cases, with apparent smaller sizes for the Ni-doped antimonide compared to the other two compounds.

Table 1: Summary of the main structural and microstructural features of the sintered skutterudite pellets used for the thermoelectric characterizations

| Nominal composition | $a$ [Å] | Impurity [wt.%] | Average grain size [nm] | Relative density [%] |
|---|---|---|---|---|
| $CoSb_3$ | 9.0362(4) | None | $784 \pm 376$ | 96 |
| $Ni_{0.06}Co_{0.94}Sb_3$ | 9.0428(3) | None | $580 \pm 336$ | 97 |
| $In_{0.13}Co_4Sb_{12}$ | 9.0482(3) | Sb (<1) | $617 \pm 292$ | 97 |

In order to quantify these observations, image analyses were performed using the *Channel 5* software (HKL Technology) by considering all the diffracting domains containing at least 7 pixels (*i.e.* $\sim$0.07 $\mu$m$^2$) for $CoSb_3$ and $In_{0.13}Co_4Sb_{12}$ and at least 14 pixels (*i.e.* $\sim$0.035 $\mu$m$^2$) for $Ni_{0.06}Co_{0.94}Sb_3$. The particles size distribution (diameter of an equivalent circle with equal surface, Fig. 5) clearly shows a majority of submicronic particles. This distribution has been fitted using a log-normal distribution function:

$$f(x) = \frac{A}{x\sigma\sqrt{2\pi}}.exp(-\frac{[ln(x)-\mu]^2}{2\sigma^2}) \quad (3)$$

where $A$, $\mu$ and $\sigma$ are the fitting parameters. From $\mu$ and $\sigma$ values, the average grain size D and its standard deviation SD can be calculated using the formulae:

$$D = exp(\mu + \frac{\sigma^2}{2}) \quad (4)$$

$$SD = [(exp(\sigma^2)-1).exp(2\mu+\sigma^2)]^{\frac{1}{2}} \quad (5)$$

The average grain sizes are found to range from 780 nm for $CoSb_3$ down to 580 nm for $Ni_{0.06}Co_{0.94}Sb_3$ with intermediate values for the In-inserted phase (Table 1).

Such small grain sizes induce numerous grain boundaries, which along the presence of defects due to crystal orientation mismatches might be efficient to

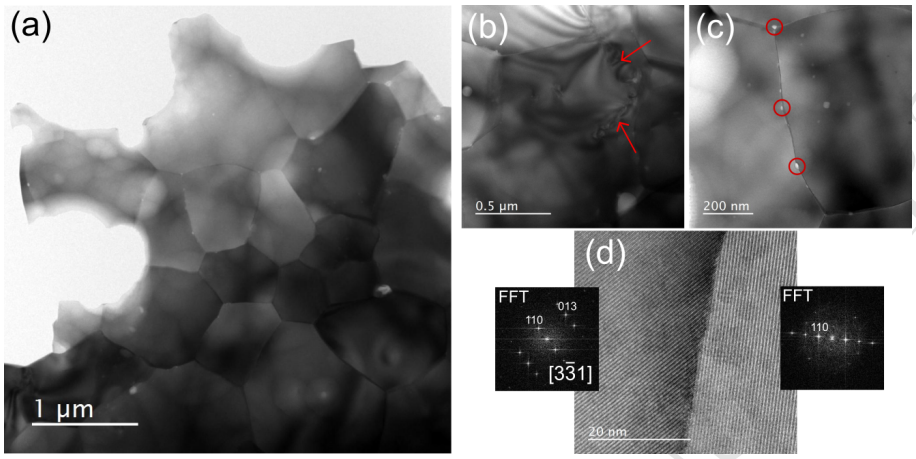


Fig. 6: TEM brightfield images of thinned $CoSb_3$ sintered pellet. (a) Typical global area, (b) strips indicating lattice distortions originating from dislocations high density at the grain boundaries (red arrows), (c) nano-scale porosities (encircled in red) and (d) HRTEM image showing the crystallinity of the grain boundaries

decrease the lattice thermal conductivity. It was shown that dislocations or nanoscale porosity/precipitate can efficiently reduce the skutterudites thermal conductivity by phonon scattering [30, 59, 60]. In order to demonstrate the existence of such defects in our materials, $CoSb_3$ sintered pellet grains boundaries have been investigated by TEM. Fig. 6a shows a typical area of the thinned pellet where the observations were realized. At this magnification, proper tilting of the sample reveals stripes originating from boundaries and propagating inside the grains (Fig. 6b). Contrast between those stripes arises from slight deviation from the diffraction condition and evidences large lattice constraints in the crystal. These are common to sintered materials as they originate from high density of dislocations, which are in the present case, mostly located close to or at the grain boundaries (red arrows). HRTEM examination of such grain boundaries (Fig. 6d and SI.5) reveals that they are well-crystallized and free of any amorphous layer. Two major kinds of defects are evidenced in Fig. SI.5 taken on a semi-coherent lattice interface. Typical dislocations appear inside the grains (Fig. SI.5b) while two dimensional analogues of dislocations [61] are created at the interface between the grains (Fig. SI.5c), both types being

able to scatter mid-wavelength phonons.

As shown in Fig. 6c, some porosity with nanometric size (encircled in red) is also observed at the grain boundaries and can also act as efficient phonon scattering centers.

All these observations are quite common for sintered materials and are not a special feature resulting from the magnesioreduction synthesis. However, an exacerbated effect on the thermal conductivity is expected in MR-materials because of the high grain boundary concentration leading to an elevated defect concentration.

## 3.2. Thermoelectric characterizations

The electrical resistivities, Seebeck coefficients and thermal conductivities have been determined in the temperature range 300-800 K where skutterudites usually present their maximum *ZT* value.

The electrical resistivity and Seebeck coefficient of the three pellets are shown in Fig. 7a and 7b. $CoSb_3$ shows a semiconducting shape of $\rho(T)$ in the 300-800 K temperature range and the $\alpha(T)$ evolves from strongly negative at room temperature to positive at 800 K with a sign change at 600 K attributed to the intrinsic regime caused by holes activation through the band gap [62, 63, 43]. The electrical resistivity of the Ni-doped and In-inserted skutterudites are strongly reduced to respectively 14.5 and 16.0 $\mu\Omega$.m at 300 K confirming the insertion of these elements in the crystal structure. The *n*-doping is confirmed by the stabilized negative value of $\alpha(T)$ in both cases, ranging between -120 and -200 $\mu$V K$^{-1}$ for $Ni_{0.06}Co_{0.94}Sb_3$ and between -180 and -240 $\mu$V K$^{-1}$ for $In_{0.13}Co_4Sb_{12}$ in the investigated temperature range. The electrical resistivities and Seebeck coefficients are in very good agreement with those reported for similar compositions of Ni-doped [41, 64] and In-filled [44, 65] $CoSb_3$. These values lead to an increase of the maximum *PF* (Fig. 7c) from about 1 mW m$^{-1}$ K$^{-2}$ at 400 K for $CoSb_3$ to 3 and 3.5 mW m$^{-1}$ K$^{-2}$ for $Ni_{0.06}Co_{0.94}Sb_3$ at 700 K and $In_{0.13}Co_4Sb_{12}$ at 600 K, respectively. The small grain sizes and

thus a high concentration of grain boundaries do not seem to alter the sample transport properties that are dominated by the high crystallinity of the powder particles.

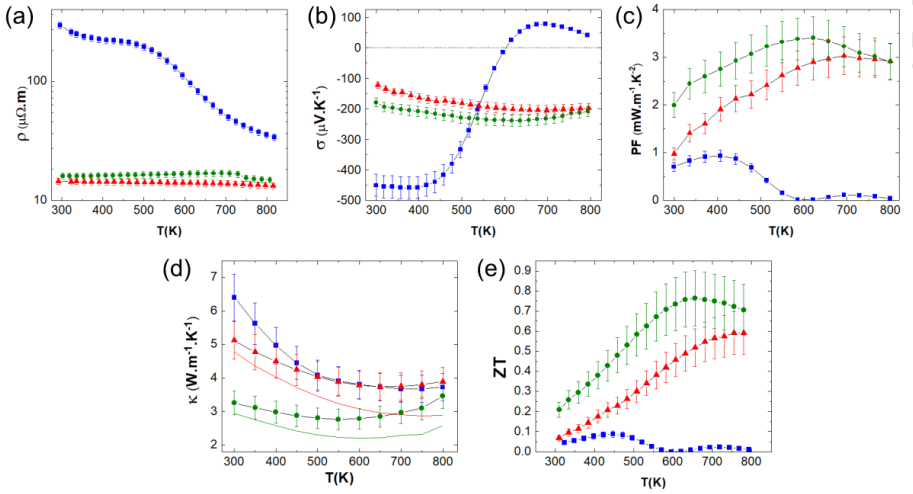


Fig. 7: High-temperature dependence of (a) the electrical resistivity, (b) Seebeck coefficient, (c) power factor, (d) total (symbols) and lattice (solid colored lines) thermal conductivity and (d) figure-of-merit *ZT* of ( ■ ) $CoSb_3$, ( ▲ ) $Ni_{0.06}Co_{0.94}Sb_3$ and ( ● ) $In_{0.13}Co_4Sb_{12}$. Standard deviations have been estimated to 6 %, 8 %, 13 %, 11 % and 18 % for electrical resistivity, Seebeck coefficient, power factor, thermal conductivity and figure-of-merit *ZT*, respectively, according to [66]

Table 2: Measured total thermal conductivity and calculated lattice thermal conductivity in W $m^{-1}$ $K^{-1}$ of $CoSb_3$, $Ni_{0.06}Co_{0.94}Sb_3$ and $In_{0.13}Co_4Sb_{12}$ at 300 K and 800 K compared to the thermal conductivities of macrostructured compounds with similar compositions reported in literature.

| | | MR samples | | Literature data | |
|---|---|---|---|---|---|
| | | 300 K | 800 K | 300 K | 800 K (700 K*) |
| $CoSb_3$ | $\kappa$ | 6.5 | 3.7 | 11.1 [43], 9.2 [44] | 7.5* [43], 4.9 [44] |
| | $\kappa_L$ | 6.5 | 3.4 | 11.1 [43], 9.0 [44] | 7.2* [43], 4.6 [44] |
| $Ni_{0.06}Co_{0.94}Sb_3$ | $\kappa$ | 5.1 | 3.9 | 6.7 [41] | 4.4 [41] |
| | $\kappa_L$ | 4.7 | 2.9 | 6.3 [41] | 3.4 [41] |
| $In_{0.13}Co_4Sb_{12}$ | $\kappa$ | 3.3 | 3.5 | 3.5 [44], 4.6 [65] | 3.0 [44], 3.2* [65] |
| | $\kappa_L$ | 2.9 | 2.6 | 3.1 [44], 3.9 [65] | 2.3 [44], 2.5*[65] |

The thermal diffusivity of the three synthesized skutterudites has been measured on sintered pellets and converted to thermal conductivity (Fig. 7d) using

the densities of the pellets and the Dulong and Petit specific heat which usually applies for skutterudites in this temperature range. The overall shape of $\kappa(T)$ for pristine $CoSb_3$ corresponds to that usually reported for this material [44]. Nevertheless, it ranges from 6.5 W m$^{-1}$ K$^{-1}$ at 300 K down to 3.7 W m$^{-1}$ K$^{-1}$ at 800 K. Values reported for similar materials which were synthesized by conventional melting-annealing routes and being mostly composed of crytallites much larger than 1 $\mu$m are between 9-11 down to 5-7.5 W m$^{-1}$ K$^{-1}$ at 300 K and 700 K, respectively [44, 43, 64]. This corresponds to a reduction of the thermal conductivity of at least 25 % on the whole temperature range for the metalloreduced samples. The here presented values are in better agreement with those observed for 'nano'-engineered materials with comparable densities [67, 68]. A direct correlation can be made between the decrease of the thermal conductivity measured for $CoSb_3$ and the high concentration of grain boundaries and associated defects which were evidenced by EBSD/SEM and TEM analyses and act as efficient phonons scattering centers.

Because of the larger electronic contribution to the total thermal conductivity in the Ni-doped and In-filled samples and to compare more significantly with literature data, the lattice thermal conductivities $\kappa_L$ were calculated by subtracting $\kappa_e$ to $\kappa_{tot}$ (Table 2 and solid lines in Fig. 7d). The Wiedmann-Franz law, $\kappa_e$=LT/$\rho$, was used to obtain $\kappa_e$ using the measured electrical resistivity and a Lorenz number of $1.6\times10^{-8}$ and $1.7\times10^{-8}$ W $\Omega$ K$^{-2}$ for $Ni_{0.06}Co_{0.94}Sb_3$ and $In_{0.13}Co_4Sb_{12}$, respectively [41, 44].

The total thermal conductivity of $Ni_{0.06}Co_{0.94}Sb_3$ is 20 % lower than that of pristine $CoSb_3$ at 300 K and reaches similar values from 450 up to 800 K. This reduction of $\kappa(T)$ at room temperature could be explained (i) by the smaller particle size and thus higher density of grain boundaries and associated defects and (ii) by the higher mass fluctuation on the 'disordered' transition metal sublattice, both enhancing the scattering of phonons and decreasing $\kappa_L(T)$. The beneficial effect of the mesostructuration is more apparent when $\kappa_L$ is compared to the values reported for conventionally synthesized macrostructured materials and where a reduction of $\approx$ 25 % is noticed at 300 K (Table 2). At higher

temperature, the mesostructuration seems to become less and less efficient so that at 800 K the reduction of $\kappa_L$ falls to $\approx$ 15 %. Again, the measured trend and values are in good agreement with reported mesostructured samples with a similar doping level [41, 69].

With the insertion of indium rattlers in the structure, the total thermal conductivity of $In_{0.13}Co_4Sb_{12}$ is further lowered to 3.2 and 3.5 W m$^{-1}$ K$^{-1}$ at 300 and 800 K, respectively, with a minimum of 2.8 W m$^{-1}$ K$^{-1}$ at about 550 K. These correspond to $\kappa_L$ of 2.9 W m$^{-1}$ K$^{-1}$ at 300 K and 2.6 W m$^{-1}$ K$^{-1}$ at 800 K. Comparisons with literature data are rather difficult due to the wide span of (effective) rattler concentration and pellet densities encountered and to the relatively large standard deviations inherent to thermal diffusivity measurements. However the presently investigated sample seems to have a slighly lower $\kappa_L$ than reported value but without strong effect from the mesostructuration opposite to our observations on the two previous compositions. According to Benyahia *et al.* [70] who investigated the influence of grain size on $In_{0.25}Co_4Sb_{12}$ lattice thermal conductivity, the reduction of $\kappa_L(T)$ by mesostructuration would have a stronger effect from room temperature to $\approx$ 580 K while at higher temperature scattering by the rattler would become dominant. This could explain why magnesioreduced samples have a low $\kappa_L$ at 300 K compared to those reported in literature but is only in the average at 700 K. Furthermore, in the above mentioned article, a modified Nan and Birringer law [71, 72] was used to estimate the reduction of $\kappa_L$ according to the reciprocal of the crystallite size in $In_{0.25}Co_4Sb_{12}$ at 300 K. Applying here this law and considering a mean crystallite size of 600 nm, a reduction of $\kappa_L$(300 K) of only $\approx$ 10% is estimated compared to macrostructured materials. This must be taken as a rough estimate since the synthesis routes and the methods for grain size determination are different, but it would support the reduction of $\kappa_L(T)$ thanks to mesostructuration especially near room temperature in $In_{0.13}Co_4Sb_{12}$.

The measured physical properties enable to calculate the figure-of-merit $ZT$ of these materials (Fig. 7e). The $ZT$ values of pristine $CoSb_3$ are small due to the combined high electrical resistivity and the occurrence of the bipolar effect

around 500 K. The obtained values for the Ni-doped and In-filled $CoSb_3$ increase *ZT* up to 0.6 at 800 K and 0.75 at 650 K, respectively. In the case of Ni-doped $CoSb_3$, this result is very similar to the improved *ZT* reported for mesostructured $Ni_{0.06}Co_{0.94}Sb_3$ where the reduction of the grain sizes and consequently of the thermal conductivities was realized by high energy ball-milling [69, 41]. In the case of $In_{0.13}Co_4Sb_{12}$, the reduction of $\kappa$ by mesostructuration is less effective due to the elevated phonon diffusion by In-rattlers and the calculated *ZT* corresponds well to materials synthesized by conventional melting/annealing methods [43, 44, 65].

## 4. Conclusions

Pure, Ni-doped and In-filled $CoSb_3$ were synthesized from metal oxides in only 84 h at temperature as low as 810 K by a magnesioreduction process. As-synthesized powders are directly composed of well-crystallized submicronic particles. After spark plasma sintering, pellets with excellent purities and high densities were obtained. XRD and SEM analyses show that the dopant and rattler concentrations are very close to the targetted ones, indicating that a good control of the chemical composition is possible with this process. After sintering, the average grain size are found to be 780, 580 and 620 nm for $CoSb_3$, $Ni_{0.06}Co_{0.94}Sb_3$ and $In_{0.13}Co_4Sb_{12}$, respectively. Such small grain size along with the presence of crystal defects and nanoporosity at the grain boundaries were shown to decrease the lattice thermal conductivity of the samples especially for $CoSb_3$ and $Ni_{0.06}Co_{0.94}Sb_3$ where strong $\kappa_L$ reduction of 25 % were observed at 300 K. The electrical resistivity and Seebeck coefficient measurements show no degradation of the transport properties due to the reduction of grain sizes. This synthesis route thus directly leads to materials approaching the 'phonon glass-electron crystal' state [73]. It results in $ZT_{max}$ of 0.09 at 450 K, 0.60 at 800 K and 0.75 at 650 K for $CoSb_3$, $Ni_{0.06}Co_{0.94}Sb_3$ and $In_{0.13}Co_4Sb_{12}$, respectively. These values are close to those reported in literature for similar compositions but after multistep high temperature syntheses followed by various mesostructura-

tion steps. This industrializable process is thus promising for the preparation of thermoelectric materials and will be applied to more complex (multi-doped and -filled) skutterudites but also to other intermetallic thermoelectric materials such as clathrates, (half-)Heusler phases or transition metal silicides.

## Acknowledgements

Francis Gouttefangeas is acknowledged for SEM images and EDS analyses performed on the CMEBA platform. TEM experiments were performed on THEMIS platform. Both platforms belong to the ScanMAT unit (UMS 2001, University of Rennes 1) which received a financial support from the European Union (CPER-FEDER 2007-2014).// Laura Paradis-Fortin is acknowledged for her careful reading of the article and correction of language errors.

[1] L. Yang, Z.-G. Chen, M. S. Dargusch, J. Zou, High Performance Thermoelectric Materials: Progress and Their Applications, Adv. Energy Mater. 8 (2018) 1701797.

[2] B. C. Sales, D. Mandrus, R. K. Williams, Filled skutterudite antimonides: A new class of thermoelectric materials, Science 272 (1996) 1325–1328.

[3] G. S. Nolas, D. T. Morelli, T. M. Tritt, Skutterudites: A phonon-glass-electron crystal approach to advanced thermoelectric energy conversion applications, Annu. Rev. Mater. Sci. 29 (1999) 89–116.

[4] S. LeBlanc, S. K. Yee, M. L. Scullin, C. Dames, K. E. Goodson, Material and manufacturing cost considerations for thermoelectrics, Renew. Sust. Energ. Rev. 84 (2014) 313–327.

[5] G. Rogl, P. Rogl, Skutterudites, a most promising group of thermoelectric materials, Curr. Opin. Green Sustainable Chem. 4 (2017) 50–57.

[6] M. Puyet, C. Candolfi, L. Chaput, V. D. Ros, A. Dauscher, B. Lenoir, J. Hejtmanek, Low-temperature thermal properties of n-type partially filled calcium skutterudites, J. Phys.:Condens. Matter 18 (2006) 11301–11308.

[7] G. S. Nolas, J. Yang, H. Takizawa, Transport properties of germanium-filled $CoSb_3$, Appl. Phys. Lett. 84 (2004) 5210–5212.

[8] X. Y. Zhao, X. Shi, L. D. Chen, W. Q. Zhang, W. B. Zhang, Y. Z. Pei, Synthesis and thermoelectric properties of Sr-filled skutterudite $Sr_yCo_4Sb_{12}$, J. Appl. Phys. 99 (2006) 053711.

[9] G. Rogl, A. Grytsiv, K. Yubuta, S. Puchegger, E. Bauer, C. Raju, R. C. Mallik, P. Rogl, In-doped multifilled n-type skutterudites with ZT=1.8, Acta Mater. 95 (2015) 201–211.

[10] J. Gainza, F. Serrano-Sánchez, J. Prado-Gonjal, N. M. Nemes, N. Biskup, O. J. Dura, J. L. Martínez, F. Fauth, J. A. Alonso, Substantial thermal conductivity reduction in mischmetal skutterudites $Mm_xCo_4Sb_{12}$ prepared under high-pressure conditions, due to uneven distribution of the rare-earth elements, J. Mater. Chem. C 7 (2019) 4124–4131.

[11] K. Wojciechowski, J. Tobola, J. Leszczynski, Thermoelectric properties and electronic structure of $CoSb_3$ doped with Se and Te, J. Alloys Compd. 361 (2003) 19–27.

[12] J. Mi, X. Zhao, T. Zhu, J. Ma, Thermoelectric properties of skutterudites $Fe_xNi_yCo_{1-x-y}Sb_3$ (x=y), J. Alloys Compd. 452 (2008) 225–229.

[13] Y. Lan, A. J. Minnich, G. Chen, Z. Ren, Enhancement of Thermoelectric Figure-of-Merit by a Bulk Nanostructuring Approach, Adv. Funct. Mater. 20 (2010) 357–376.

[14] X. Meng, Z. Liu, B. Cui, D. Qin, H. Geng, W. Cai, L. Fu, J. He, Z. Ren, J. Sui, Grain Boundary Engineering for Achieving High Thermoelectric Performance in n-Type Skutterudites, Adv. Energy Mater. 7 (2017) 1602582.

[15] G. Joshi, H. Lee, Y. Lan, X. Wang, G. Zhu, D. Wang, R. W. Gould, D. C. Cuff, M. Y. Tang, M. S. Dresselhaus, G. Chen, Z. Ren, Enhanced Thermoelectric Figure-of-Merit in Nanostructured p-type Silicon Germanium Bulk Alloys, Nano Lett. 8 (2008) 4670–4674.

[16] L. Yang, Z. G. Chen, M. Hong, G. Han, J. Zou, Enhanced Thermoelectric Performance of Nanostructured $Bi_2Te_3$ through Significant Phonon Scattering, ACS Appl. Mater. Interfaces 7 (2015) 23694–23699.

[17] C. Recknagel, N. Reinfried, P. H*ö*hn, W. Schnelle, H. Rosner, Y. Grin, A. Leithe-Jasper, Application of spark plasma sintering to the fabrication of binary and ternary skutterudites, Sci. Tech. Adv. Mater. 8 (2007) 357–363.

[18] V. Trivedi, M. Battabyal, P. Balasubramanian, G. M. Muralikrishna, P. K. Jain, R. Gopalan, Microstructure and doping effect on the enhancement of the thermoelectric properties of Ni doped Dy filled $CoSb_3$ skutterudites, Sustain. Energ. Fuels 2 (2018) 2687–2697.

[19] G. Rogl, A. Grytsiv, R. Anbalagan, J. Bursik, M. Kerber, E. Schafler, M. Zehetbauer, E. Bauer, P. Rogl, Direct SPD-processing to achieve high-ZT skutterudites, Acta Mater. 159 (2018) 352–363.

[20] L. Guo, G. Wang, K. Peng, Y. Yan, X. Tang, M. Zeng, J. Dai, G. Wangand, X. Zhou, Melt spinning synthesis of p-type skutterudites: Drastically speed up the process of high performance thermoelectrics, Scipta Mater. 116 (2016) 26–30.

[21] S. Lee, K. H. Lee, Y.-M. Kim, H. S. Kim, G. J. Snyder, S. Baik, S. W. Kim, Simple and efficient synthesis of nanograin structured single phase filled skutterudite for high thermoelectric performance, Acta. Mater. 142 (2018) 8–17.

[22] E. Godlewska, K. Mars, K. Zawadzka, Alternative route for the preparation of $CoSb_3$ and $Mg_2Si$ derivatives, J. Solid State Chem. 193 (2012) 109–113.

[23] F. Gucci, T. G. Saunders, M. J. Reece, In-situ synthesis of n-type unfilled skutterudite with reduced thermal conductivity by hybrid flash-spark plasma sintering, Scripta Mater. 157 (2018) 58–61.

[24] L. Kong, X. Jia, Y. Zhang, B. Sun, B. Liu, H. Liu, C. Wang, B. Liu, J. Chen, H. Ma, N-type $Ba_{0.3}Ni_{0.15}Co_{3.85}Sb_{12}$ skutterudite: High pressure processing

technique and thermoelectric properties, J. Alloys Compd. 734 (2018) 36–42.

[25] L. Deng, J. Ni, L. Wang, X. Jia, J. Qin, B. Liu, Structure and thermoelectric properties of $In_xBa_yCo_4Sb_{12}$ samples prepared by HPHT, J. Alloys Compd. 712 (2017) 477–481.

[26] A. Sesselmann, G. Skomedal, H. Middleton, E. M*ü*ller, The Influence of Synthesis Procedure on the Microstructure and Thermoelectric Properties of p-Type Skutterudite $Ce_{0.6}Fe_2Co_2Sb_{12}$, J. Electron. Mater. 45 (2015) 1397–1407.

[27] M. S. Toprak, C. Stiewe, D. Platzek, S. Williams, L. Bertini, E. M*ü*ller, C. Gatti, Y. Zang, M. Rowe, M. Muhammed, The impact of nanostructuring on the thermal conductivity of thermoelectric $CoSb_3$, Adv. Funct. Mater. 14 (2004) 1189–1196.

[28] Y. Li, C. Li, B. Wang, W. Li, P. Che, A comparative study on the thermoelectric properties of $CoSb_3$ prepared by hydrothermal and solvothermal route, J. Alloys Compd. 772 (2019) 770–774.

[29] K. Biswas, J. He, I. D. Blum, C.-I. Wu, T. P. Hogan, D. N. Seidman, V. P. Dravid, M. G. Kanatzidis, High-performance bulk thermoelectrics with all-scale hierarchical architectures, Nature 489 (2012) 414–418.

[30] X. Meng, Z. Liu, B. Cui, D. Gin, H. Geng, W. Cai, L. Fu, J. He, Z. Ren, J. Sui, Grain Boundary Engineering for Achiving High Thermoelectric Performance in n-Type Skutterudite, Adv. Energy Mater. 7 (2017) 642–651.

[31] W. Li, J. Wang, Y. Xie, J. L. Gray, J. J. Heremans, H. B. Kang, B. Poudel, S. T. Huxtable, S. Priya, Enhanced thermoelectric performance of Yb-single-filled skutterudite by ultralow thermal conductivity, Chem. Mater. 31 (2019) 862–872.

[32] G. Rogl, A. Grytsiv, P.Rogl, E. Bauer, M. B. Kerber, M. Zehetbauer, S. Puchegger, Multifilled nanocrystalline p-type didymium-Skutterudites with ZT>1.2, Intermetallics 18 (2010) 2435–2444.

[33] M. Matsubara, Y. Masuoka, R. Asahi, Effects of doping IIIB elements (Al, Ga, In) on thermoelectric properties of nanostructured n-type filled skutterudite compounds, J. Alloys Compd. 774 (2019) 731–738.

[34] H. Yang, P. Wen, X. Zhou, Y. Li, B. Duan, P. Zhai, Q. Zhang, Enhanced thermoelectric performance of Te-doped skutterudite with nano-micro-porous architecture, Scripta Mater. 159 (2018) 68–71.

[35] A. U. Khan, K. Kobayashi, D.-M. Tang, Y. Yamauchi, K. Hasegawa, M. Mitome, Y. Xue, B. Jiang, K. Tsuchiya, D. Golberg, Y. Bando, T. Mori, Nano-micro-porous skutterudites with 100% enhancement in ZT for high performance thermoelectricity, Nano Energy 31 (2017) 152–159.

[36] H. Li, X. Su, X. Tang, Q. Zhang, C. Uher, G. J. Snyder, U. Aydemir, Grain boundary engineering with nano-scale InSb producing highperformance $In_xCe_yCo_4Sb_{12+z}$skutterudite thermoelectrics, J. Materiomics 3 (2017) 273–279.

[37] P. Chen, Z. Zhou, W. Jiang, WeiLuo, J. Yang, J. Zhu, L. Wang, Y. Fan, Enhancing the thermoelectric performance of filled skutterudite nanocomposites in a wide temperature range via electroless silver plating, Scripta Mater. 146 (2018) 136–141.

[38] H. Zhao, B. Cao, S. Li, N. Liu, J. Shen, S. Li, J. Jian, L. Gu, Y. Pei, G. J. Snyder, Z. Ren, X. Chen, Engineering the Thermoelectric Transport in Half-Heusler Materials through a Bottom-Up Nanostructure Synthesis, Adv. Energy Mater. 7 (2017) 1700446.

[39] L. Ma, C. Y. Seo, X. Chen, K. Sun, J. W. Schwank, Indium-doped $Co_3O_4$ nanorods for catalytic oxidation of CO and $C_3H_6$ towards diesel exhaust, Appl. Catal. B-Environ. 222 (2018) 44–58.

[40] E. Alleno, E. Zehani, O. Rouleau, Metallurgical and thermoelectric properties in $Co_{1-x}Pd_xSb_3$ and $Co_{1-x}Ni_xSb_3$ revisited, J. Alloys Compd. 572 (2013) 43–48.

[41] E. Alleno, E. Zehani, M. Gaborit, V. Orodniichuk, B. Lenoir, M. Benyahia, Mesostructured thermoelectric $Co_{1-y}M_ySb_3$ (M = Ni, Pd) skutterudites, J. Alloys Compd. 692 (2017) 676–686.

[42] T. He, J. Chen, H. D. Rosenfeld, M. A. Subramanian, Thermoelectric properties of indium-filled skutterudites, Chem. Mater. 18 (2006) 759–762.

[43] R. C. . Mallik, J. Y. Jung, S. C. Ur, I. H. Kim, Thermoelectric properties of $In_zCo_4Sb_{12}$ skutterudites, Met. Mater. Int. 14 (2008) 223–228.

[44] J. Leszczynski, V. D. Ros, B. Lenoir, A. Dauscher, C. Candolfi, P. Masschelein, J. Hejtmanek, K. Kutorasinski, J. Tobola, R. I. Smith, C. Stiewe, E. M*ü*ller, Electronic band structure, magnetic, transport and thermodynamic properties of In-filled skutterudites $In_xCo_4Sb_{12}$, J. Phys. D: Appl. Phys. 46 (2013) 495106.

[45] R. C. Mallik, C. Stiewe, G. Karpinski, R. Hassdorf, E. Müller, Thermoelectric properties of $Co_4Sb_{12}$ skutteurdite materials with partial In filling and excess In additions, J. Electron. Mater. 38 (2009) 1337–1339.

[46] G. Li, K. Kurosaki, Y. Ohishi, H. Muta, S. Yamanaka, Thermoelectric properties on Indium-added skutteurdites $In_XCo_4Sb_{12}$, J. Electron. Mater. 42 (2013) 1463–1468.

[47] E. Visnow, C. P. Heinrich, A. S. andJ. de Boor, P. Leidich, B. Klobes, R. P. Hermann, W. E. Müller, W. Tremel, On the true Indium content on In-filled skutterudites, Inorg. Chem. 54 (2015) 7818–7827.

[48] J. Rodriguez-Carvajal, Recent advances in magnetic-structure determination by neutron powder diffraction, Physica B 192 (1993) 55–69.

[49] O. Rouleau, E. Alleno, Measurement system of the Seebeck coefficient or of the electrical resistivity at high temperature, Rev. Sci. Instrum. 84 (2013) 105103.

[50] D. G. Mandrus, A. Migliori, T. W. Darling, M. F. Hundley, E. J. Peterson, J. D. Thompson, Electronic transport in lightly doped $CoSb_3$, Phys. Rev. B 52 (1995) 4926–4931.

[51] M. Christensen, B. B. Iversen, L. Bertini, C. Gatti, M. Toprak, M. Muhammed, E. Nishibori, Structural study of Fe doped and Ni substituted thermoelectric skutterudites by combined synchrotron and neutron powder diffraction and *ab inition* theory, J. Appl. Phys. 96 (2004) 3148–3157.

[52] W. Zhao, P. Wei, Q. J. Zhang, H. Peng, W. T. Zhu, D. G. Tang, J. Yu, H. Y. Zhou, Z. Y. Liu, X. Mu, D. Q. He, J. C. Li, C. L. Wang, X. F. Tang, J. H. Yang, Multi-localization transport behaviour in bulk thermoelectric materials, Nat. Commun. 6 (2015) 6197.

[53] A. Grytsiv, P. Rogl, H. Michor, E. Bauer, G. Giester, $In_yCo_4Sb_{12}$ Skutterudite: Phase Equilibria and Crystal Structure, J. Electron. Mater. 42 (2013) 2940–2952.

[54] G. Champion, J. Allenou, M. Pasturel, H. Noël, F. Charollais, M. Anselmet, X. Iltis, O. Tougait, Magnesiothermic Reduction Process Applied to the Powder Production of U(Mo) Fissile Particles, Adv. Eng. Mater. 15 (2013) 257–261.

[55] K. Choi, H. Choi, H. Na, I. Sohn, Effect of magnesium on the phase equilibria in magnesio-thermic reduction of $Nb_2O_5$, Mater. Lett. 183 (2016) 151–155.

[56] C. Won, H. Nersisyan, H. Won, Titanium powder prepared by a rapid exothermic reaction, Chem. Eng. J. 157 (2010) 270–275.

[57] H. J. T. Ellingham, Reducibility of oxides and sulfides in metallurgical processes, J. Soc. Chem. Ind. 63 (1944) 125–160.

[58] R. C. Sharma, T. L. Ngai, Y. A. Chang, The In-Sb (Indium-Antimony) system, Bull. Alloy Phase Diagrams 10 (1989) 657–664.

[59] G. Rogl, A. Grytsiv, P. Rogl, E. Royanian, E. Bauer, J. Horky, D. Setman, E. Schafler, M. Zehetbauer, Dependence of thermoelectric behaviour on severe plastic deformation parameters: A case study on p-type skutterudite $DD_{0.60}Fe_3CoSb_{12}$, Acta. Mater. 61 (2013) 6778–6789.

[60] L. Yang, J. Wu, L. Zhang, Synthesis of filled skutterudite compound $La_{0.75}Fe_3CoSb_{12}$ by spark plasma sintering and effect of porosity on thermoelectric properties, J. Alloys Compd. 364 (2004) 83–88.

[61] J. Friedel, Dislocations, 1st Edition, Pergamon Press, 1964 (1964).

[62] Y. Kawaharada, K. Kurosaki, M. Uno, S. Yamanaka, Thermoelectric properties of $CoSb_3$, J. Alloys Compd. 315 (2001) 193–197.

[63] J. W. Sharp, E. C. Jones, R. K. Williams, P. M. Martin, B. C. Sales, Thermoelectric properties of $CoSb_3$ and related alloys, J. Appl. Phys. 78 (1995) 1013–1018.

[64] H. Kitagawa, M. Wakatsuki, H. Nagaoka, H. Noguchi, Y. Isoda, K. Hasezaki, Y. Noda, Temperature dependence of thermoelectric properties of Ni-doped $CoSb_3$, J. Phys. Chem. Solid. 66 (2005) 1635–1639.

[65] A. Sesselmann, B. Klobes, T. Dasgupta, O. Gourdon, R. Hermann, E. Müller, Neutron diffraction and thermoelectric properties of indium filled $In_xCo_4Sb_{12}$ (x=0.05, 0.2) and indium cerium filled $Ce_{0.05}In_{0.1}Co_4Sb_{12}$ skutterudites, Phys. Stat. Sol. A 213 (2016) 766–773.

[66] E. Alleno, D. Berardan, C. Byl, C. Candolfi, R. Daou, R. Decourt, E. Guilmeau, S. Hebert, J. Hejtmanek, B. Lenoir, P. Masschelein, V. Ohorodnichuk, M. Pollet, S. Populoh, D. Ravot, O. Rouleau, M. Soulier,

A round robin test of the uncertainty on the measurement of the thermoelectric dimensionless figure of merit of $Co_{0.97}Ni_{0.03}Sb_3$, Rev. Sci. Instrum. 86 (2015) 011301.

[67] E. Alleno, L. Chen, Chubilleau, B. Lenoir, O. Rouleau, M. Trichet, B. Villeroy, Thermal Conductivity Reduction in $CoSb_3$-$CeO_2$ Nanocomposites, J. Electron. Mater. 39 (2010) 1966–1970.

[68] A. Khan, M. Saleemi, M. Johnsson, L. Han, N. Nong, M. Muhammed, M. Toprak, Fabrication, spark plasma consolidation, and thermoelectric evaluation of nanostructured $CoSb_3$, J. Alloys Compd. 612 (2014) 293–300.

[69] Q. He, Q. Hao, X. Wang, J. Yang, Y. Lan, X. Yan, B. Yu, Y. Ma, B. Poude, G. Joshi, D. Wang, G. Chen, Z. Ren, Nanostructured Thermoelectric Skutterudite $Co_{1-x}Ni_xSb_3$ Alloys, J. Nanosci. Nanotechnol. 8 (2008) 4003–4006.

[70] M. Benyahia, V. Ohorodniichuk, E. Leroy, A. Dauscher, B. Lenoir, E. Alleno, High thermoelectric figure of merit in mesostructured $In_{0.25}Co_4Sb_{12}$ n-type skutterudite, J. Alloys Compd. 735 (2018) 1096–1104.

[71] C. W. Nan, R. Birringer, Determining the Kapitza resistance and the thermal conductivity of polycrystals: A simple model, Phys. Rev. B 14 (1998) 8264–8268.

[72] H. S. Yang, G. Bai, L. Thompson, J. Eastman, Interfacial thermal resistance in nanocrystalline yttria-stabilized zirconia, Acta Mater. 50 (2002) 2309–2317.

[73] G. A. Slack, Design Concepts for Improved Thermoelectric Materials, MRS Proceedings 478 (1997) 47.

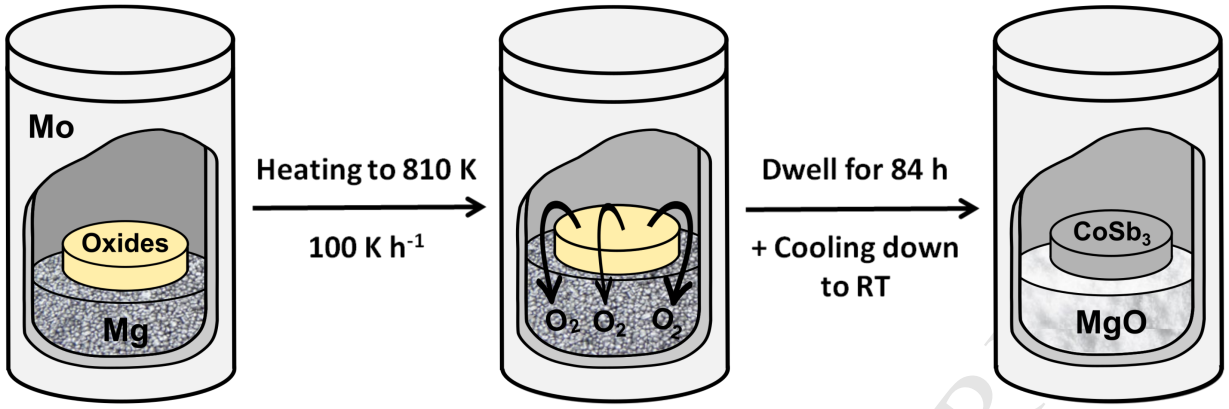

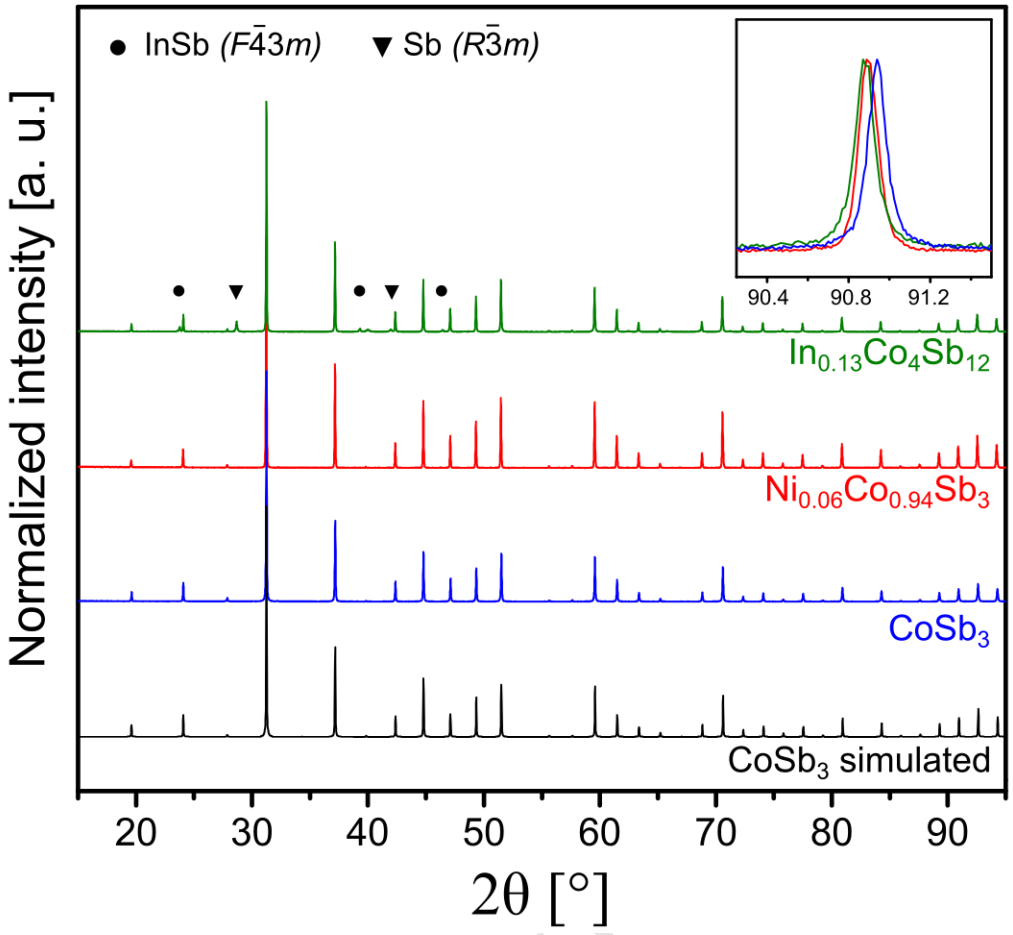

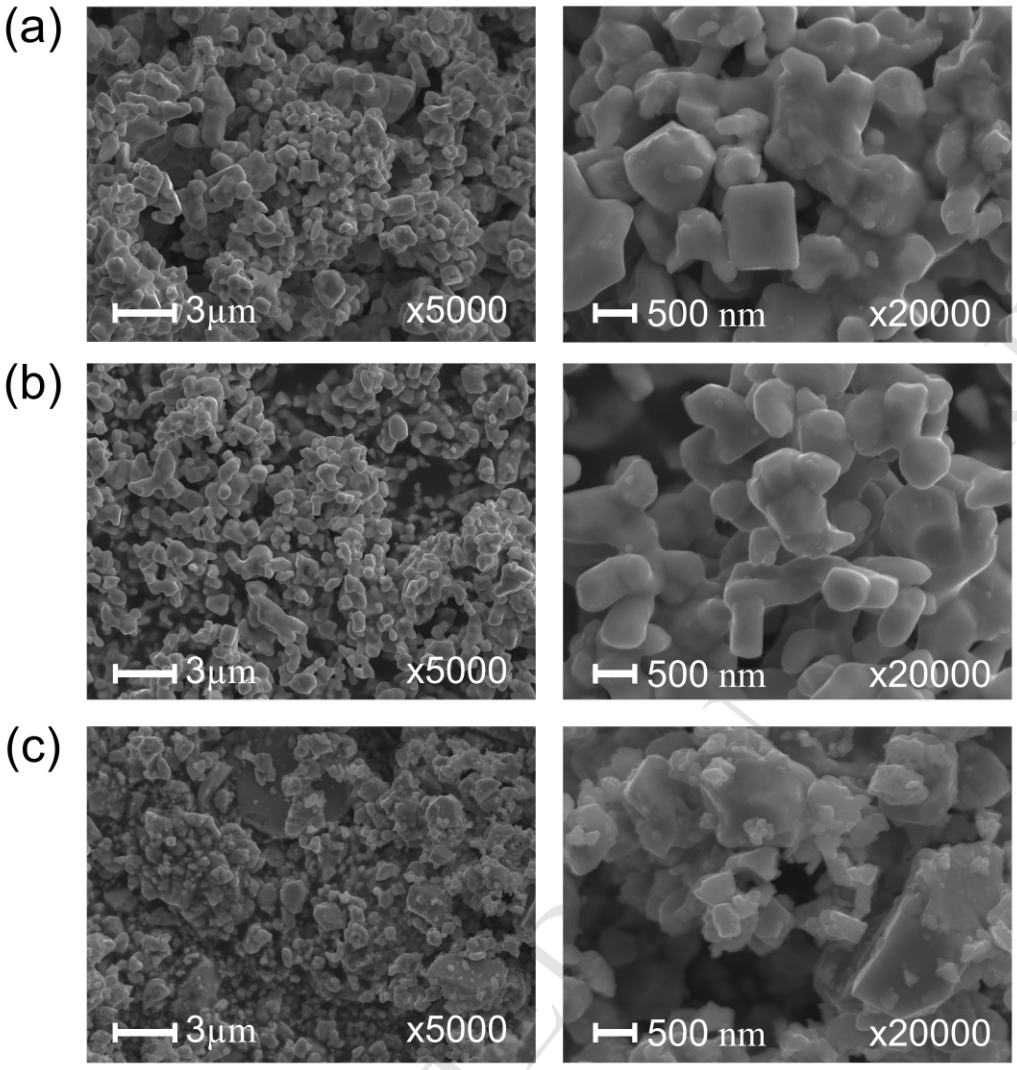

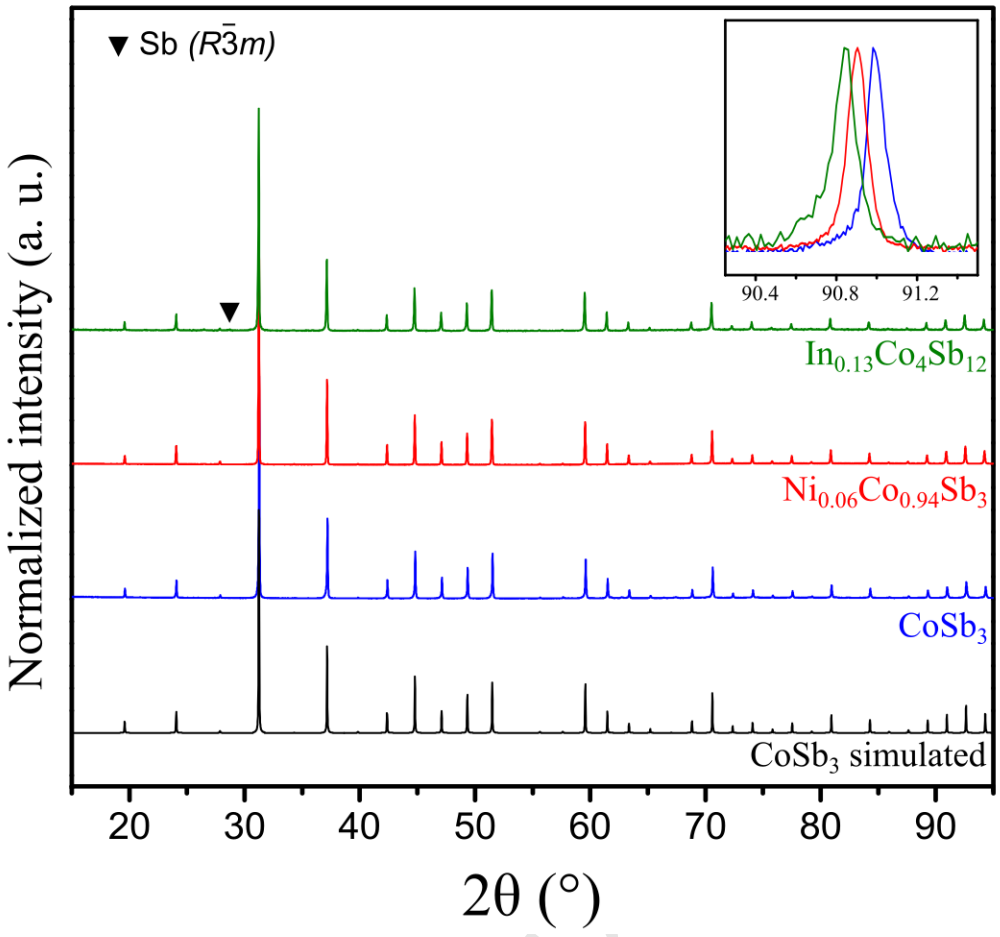

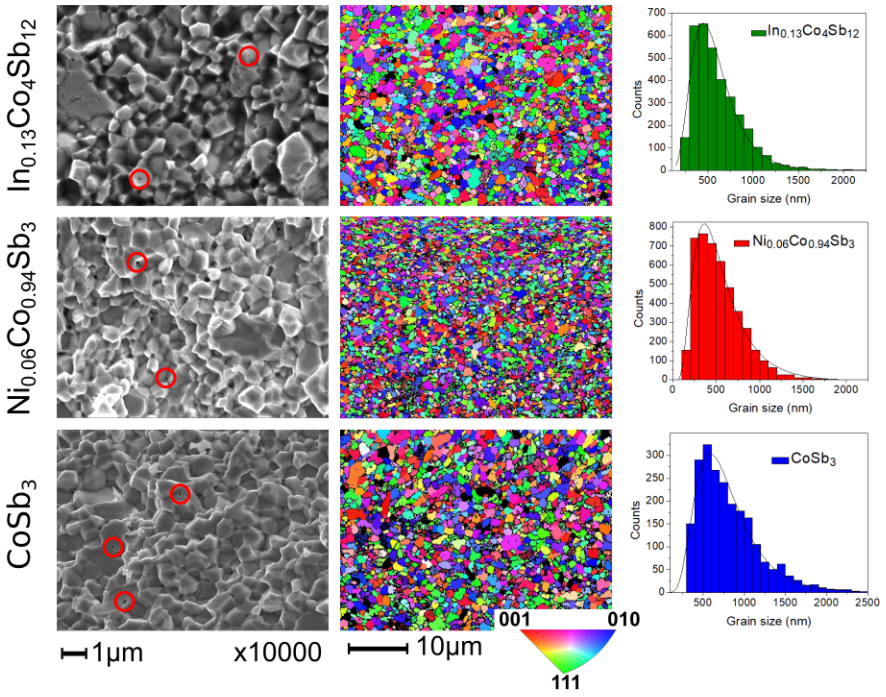

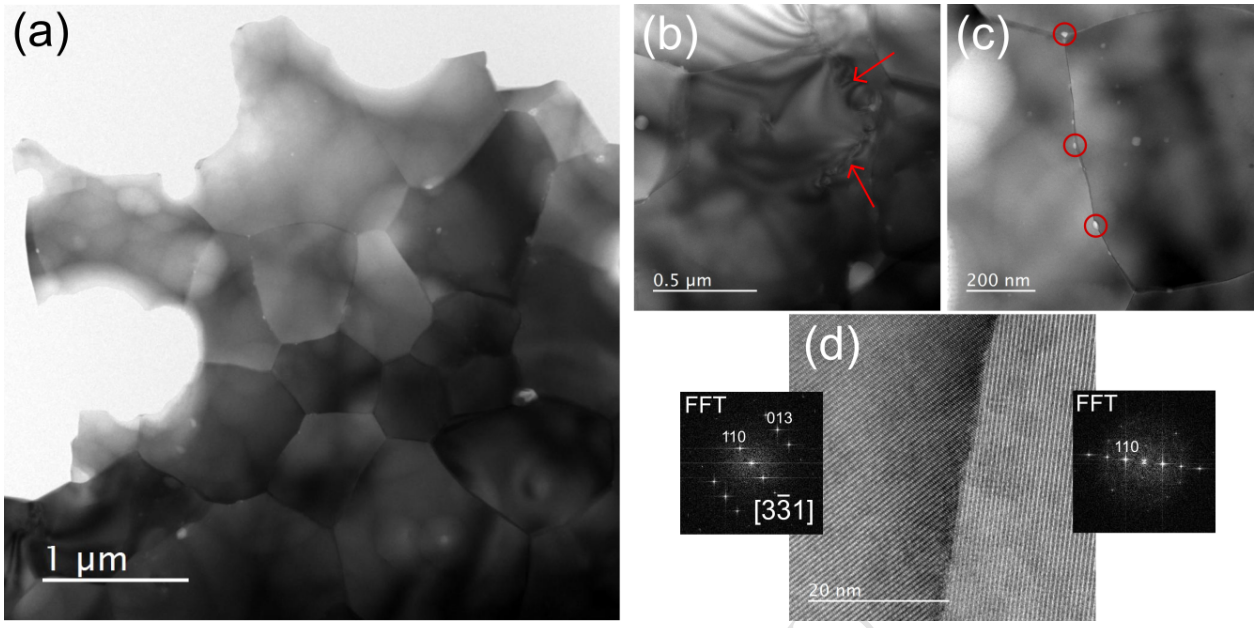

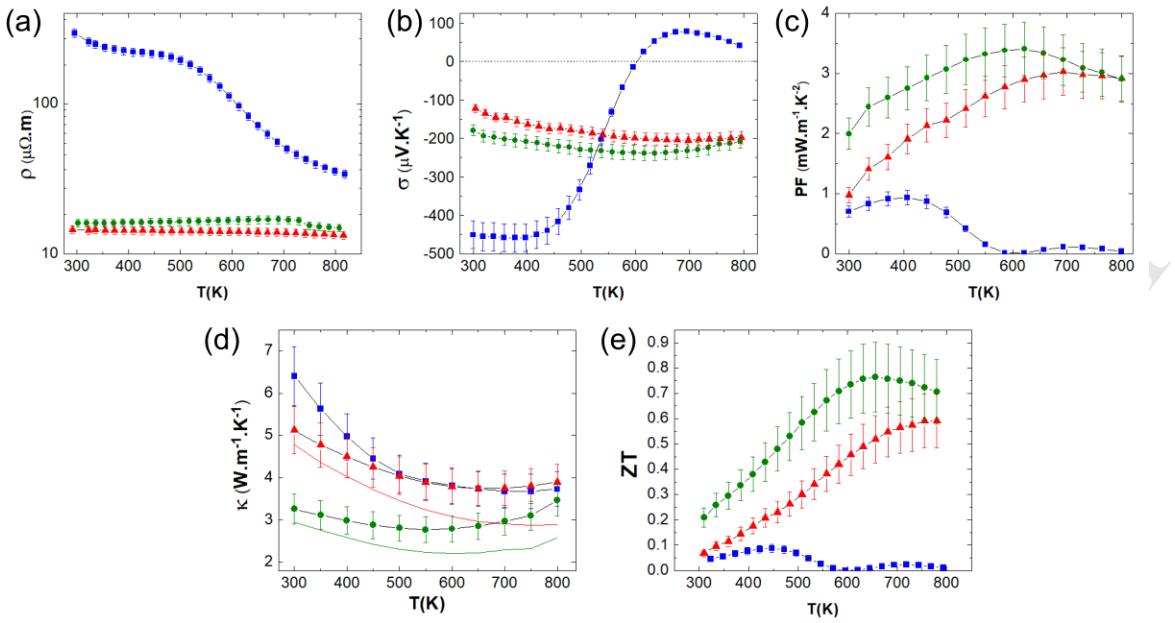

- Magnesioreduction of oxides is used to prepare skutterudites.
- Well-crystallized and submicronic powders are obtained at low temperature.
- The mesostructuration survives after spark plasma sintering.
- Accordingly, improved thermoelectric performances are achieved.
- Thermoelectric properties are discussed toward microstructure of the materials.